HIGH-RATE, REGIONAL MECHANICAL PROPERTIES OF THE PORCINE BRAIN: CROSS-COMPARISON WITH TWO METHODS OF INDENTATION

Benjamin S. Elkin, Ashok Ilankovan, Barclay Morrison III
Department of Biomedical Engineering, Columbia University, New York, NY, USA

ABSTRACT

Linear viscoelastic parameters were fit to stress relaxation data at ~10% strain, which differed significantly by anatomic region. In the corona radiata, reduced relaxation functions for strains of 10%, 20%, and 30% were not significantly different suggesting that quasilinear viscoelastic theory may be appropriate. In a second set of studies with the atomic force microscope, frequency and depth-dependent moduli were calculated from oscillatory tests in the corona radiata (5-400 Hz). Results from both methods were compared by correspondence principles and were within a factor of 3 of each other. These data, for the first time, describe high rate, large deformation behavior of multiple regions of the porcine brain which will be useful for understanding brain injury biomechanics at a finer spatial resolution than previously possible.

Keywords: Anatomy, biomechanics, brains, deformations, viscoelasticity

TRAUMATIC BRAIN INJURY (TBI) is a major cause of morbidity and mortality worldwide (Hyder et al., 2007). Development of improved treatment strategies for TBI however have stagnated (Menon, 2009), putting a stronger emphasis on injury prevention research. A better understanding of TBI biomechanics will lead to better safety systems (i.e. helmets and vehicular restraints).

Fundamental to understanding TBI biomechanics is a description of the mechanical behavior of the different anatomic regions of the brain at loading rates (>10 s^{-1}) and magnitudes (>5%) relevant to TBI (Kleiven and Hardy, 2002). While few studies have examined the mechanical properties of human brain (Ommaya, 1968; Fallenstein et al., 1969; Shuck and Advani, 1972; Pamidi and Advani, 1978; Donnelly and Medige, 1997; Prange and Margulies, 2002), porcine brain has been used as a substitute due to its gyrencephalic structure, anatomic similarity to human brain, and purported similar mechanical properties (Prange and Margulies, 2002). Multiple studies have examined the dynamic mechanical properties of porcine brain tissue (for reviews, see Nicolle et al., 2005; Cheng et al., 2008; Hrapko et al., 2008a; van Dommelen et al., 2010) with results for complex shear moduli varying from 0.1 to 10 kPa. Limitations in many of these studies include at least one of the following: (1) measurement of tissue under non-physiologic conditions (i.e. not immersed in aqueous medium) and at long or uncertain post-mortem times, (2) few anatomic regions measured, (3) no cross validation of tissue properties using different methods, (4) either loading rates or loading magnitudes not relevant to TBI.

In this study, we address these limitations by examining the mechanical properties of multiple anatomic regions in fresh porcine brain tissue maintained under physiologic conditions using two distinct modalities of measurement: a microindentation stress relaxation method and an atomic force microscope (AFM) extended to perform oscillatory loading tests. Both of these methods generated high spatial resolution mechanical property data at rates and magnitudes of deformation relevant to TBI. Shear modulus from both methods was cross-validated using correspondence principles.

METHODS:

TISSUE HARVEST: All animal procedures were approved by the Columbia University Institutional Animal Care and Use Committee. Brains from adult Yorkshire pigs (~50 kg) were removed immediately following sacrifice in studies conducted at the Columbia University Medical Center that were unrelated to the brain. In this way, the post-mortem delay within the skull was practically eliminated, and the post-mortem time to testing was known exactly. Brains were transported in ice cold oxygenated aCSF supplemented with glucose and were dissected and plated within 1 h of sacrifice. All tests were completed within 3 h of sacrifice. For microindenter studies, 2 mm thick coronal slices were generated with a brain matrix. Slices were adhered to plastic dishes

with a thin film of cyanoacrylate glue. For AFM studies, 350 µm thick coronal slices were generated with a McIlwain tissue chopper (Harvard Apparatus). Slices were plated on plastic dishes coated with laminin (Invitrogen) and poly-L-lysine (Sigma). To maintain tissue health for both studies, slices were kept in nutrient medium at physiologic pH (CO_2-independent medium supplemented with 4 mg/ml D-glucose; Invitrogen). Slices for AFM testing were placed on a rocker for 5 minutes to remove cell debris prior to indentation tests.

MICROINDENTATION: Stress relaxation indentation tests were performed with a custom-designed microindentation device. The indentation apparatus was composed of a 250 µm radius flat cylindrical punch (National Jet Company), a 10 gram load cell (GSO-10, Transducer Techniques), and a linear actuator (M-227.10, Physik Instrumente). Load cell output and indenter displacement were digitized at 10,000 samples/s. The indenter was brought into contact with the tissue to achieve a 1mg tare load before indentation. Single step indentations were performed to a depth of 40 µm (750 µm/s nominal velocity, ~10% strain, 1.9 s^{-1} strain rate) with a 20 s hold (n>6 per region). For multi-step indentations, a second and third indentation were performed at 20 s intervals (80 µm, 20% strain and 120 µm, 30% strain). All indentation tests were performed at room temperature.

STRESS RELAXATION DATA ANALYSIS: A time-dependent shear modulus was fit to the load and displacement history using a Boltzmann hereditary integral (Radok and Lee, 1960; Sakai, 2002):

$$P(t) = \frac{4R}{1-\nu}\int_0^t G(t-\tau)\left(\frac{d\delta}{d\tau}\right)d\tau \quad (1)$$

where R was the indenter radius (250 µm), δ was indentation depth, G was shear modulus, and ν was Poisson's ratio (assumed to be 0.5; Darvish and Crandall, 2001; Lippert et al., 2004; Elkin et al., 2010) (Harding and Sneddon, 1945; Cheng et al., 2000). Using MATLAB, $G(t)$ for each region was calculated and convolved with the velocity profile of the indenter, converted to P(t), and fitted to the measured load with nlinfit.m to determine 95% confidence intervals. $G(t)$ was fit to a Prony series approximation:

$$G(t) = G_\infty + \sum_j G_j \cdot e^{-\frac{t}{\tau_j}} \quad (2)$$

where G_∞ was the equilibrium shear modulus, τ_j was the time constant for each term of exponential decay, and G_j was the associated magnitude. For the first second of relaxation, the data was weighted by the inverse of time (1/t), and for the remainder of the relaxation, to reduce processing time, the data was re-sampled with a continuously decreasing sampling rate, in which the duration between successive points was continuously increasing by 0.1 ms. Multistep indentations were analyzed by fitting Equations 1 and 2 to the load from all tests within each step thus generating a separate set of Prony series parameters for each depth of indentation. Reduced relaxation functions were generated by normalizing to the shear modulus at 10 ms, which was the time point where signal-to-noise ratio was first greater than one.

AFM INDENTATION: Dynamic AFM indentations were performed with a Bioscope AFM (Veeco) and a lock-in amplifier (SR830, Stanford Research Systems). Indentations were performed with a slow ramp indentation at 0.01 Hz (static) to acquire data at different indentation depths (0.5 to 2.5 µm) with calibrated cantilever probes (12.5µm radius spherical tips, spring constant (k) = 0.11-0.15 N/m, NovaScan). The lock-in amplifier generated a sinusoidal reference signal that superimposed small sinusoidal oscillations over the slow indentation of the probe with magnitude, a_d = 8.8 nm and frequency, ω, from 5 to 400 Hz. The magnitude and phase angle, a_r and φ, of the cantilever deflection in response to the reference driving signal were computed by the lock-in amplifier at 256 kHz. All output signals, including ramp indentation, h, were recorded at 1 kHz.

AFM DATA ANALYSIS: Contact point was identified from static deflection curves using an algorithm modeled on those of Crick and Lin (Crick and Yin, 2006; Lin et al., 2007). First, raw deflection versus displacement data was smoothed with a polynomial fit. Candidate contact points were tested by fitting data prior to the candidate contact point with a linear function and data following the contact point to a quadratic function. The contact point was identified as the point at which the sum of the mean square error (MSE) of both fits was a minimum.

The classic equation for static sample reaction force due to indentation with a spherical probe (Costa and Yin, 1999; Mattice et al., 2006) was extended to the dynamic range for the addition of the small oscillatory indentation, δ^*, by taking the first term of the Taylor expansion (Mahaffy et al., 2000; Alcaraz et al., 2002; Mahaffy et al., 2004). The total reaction force was then described in terms of both the static and oscillatory reaction forces:

$$f^*_{reaction} = f^*_{static} + f^*_{osc}$$
$$f_{static} = \frac{8}{3}\sqrt{R\delta_0^3}\,\frac{G_\infty}{(1-\nu)} \qquad (3, 4, 5)$$
$$f^*_{osc} = 4\sqrt{R\delta_0}\,\frac{G^*}{(1-\nu)}\cdot\tilde{\delta}^*$$

where G_∞ was the equilibrium shear modulus, G^* was complex shear modulus with real and imaginary (storage and loss) components, δ_0 was the static indentation depth, v was Poisson's ratio (assumed 0.5 as above), and R was probe radius (12.5 μm). Oscillatory force applied to the tissue by the cantilever was then calculated from the total response of the cantilever minus the drag force of medium on the probe:

$$f^*_{osc} = f^*_{total} - f^*_{drag}$$
$$f^*_{osc} = k\cdot\tilde{z}^*_c e^{i\omega t} - f^*_{drag} \qquad (6, 7, 8)$$
$$f^*_{osc} = ka_r e^{i\omega t}e^{-i\varphi} - i\omega\cdot\gamma\cdot\tilde{\delta}^*$$

where the viscosity term, γ, was determined from oscillations of the probe in free medium just above the tissue for every force curve. Oscillatory and static force exerted by the probe and generated by the tissue reaction ($\tilde{z}^*_c$) were equated to solve for the depth and frequency dependent static (G_∞) (Harding and Sneddon, 1945; Ting, 1966), storage (G'), and loss (G'') shear modulus:

$$G_\infty = \frac{3(1-\nu)}{8\sqrt{R\delta_o^3}}\cdot kh$$
$$G' = \frac{(1-\nu)}{4\sqrt{R\delta_o}}\cdot\frac{a_d ka_r\cos\varphi - ka_r^2}{a_d^2 - 2a_d a_r\cos\varphi + a_r^2} \qquad (9, 10, 11)$$
$$G'' = -\frac{(1-\nu)}{4\sqrt{R\delta_o}}\cdot\left[\frac{a_d ka_r\sin\varphi}{a_d^2 - 2a_d a_r\cos\varphi + a_r^2} - \omega\cdot\gamma\right]$$

Static, storage, and loss shear modulus were reported as a function of frequency and indentation depth.

CORRESPONDENCE PRINCIPLES: The shear relaxation modulus generated from microindenter stress relaxation tests in the cortical white matter was converted from the time domain to the frequency domain using the following definitions for storage and loss modulus (Findley et al., 1989):

$$G'(\omega) = G_\infty + \sum_{j=1}^{N} G_j\frac{(\omega\tau_j)^2}{1+(\omega\tau_j)^2} \qquad (12, 13)$$
$$G''(\omega) = \sum_{i=1}^{N} G_j\frac{\omega\tau_j}{1+(\omega\tau_j)^2}$$

where G_∞, G_j and τ_j were the Prony fit parameters as generated above.

Dynamic AFM data was converted from the frequency domain to the time domain by fitting Prony series parameters in Equations 12 and 13 to the storage and loss modulus measured at 1 μm and 2.5 μm depths of indentation. The number of relaxation terms, N, was allowed to vary. The following optimization function was used with fminunc.m in MATLAB to perform the fits (Baumgaertel, 1989):

$$\sum_{j=1}^{m}\left(\left[\frac{G'(\omega_j)}{\overline{G'}_j}-1\right]^2+\left[\frac{G''(\omega_j)}{\overline{G''}_j}-1\right]^2\right) \quad (14)$$

where G'_j and G''_j were the storage and loss moduli measured from AFM tests and $G'(\omega_j)$ and $G''(\omega_j)$ were calculated from Equations 12 and 13 using the fit parameters.

STATISTICS: The optimal number of time constants, τ_j, necessary to fit the relaxation response in the Prony series (Eq. 3) was determined using an F-test (Allen, 1997). Multiple comparisons of short (G_{10ms}, G_{50ms}) and long term (G_∞) shear modulus from Prony series fits were performed with Student's t-tests with Bonferroni adjusted p-values (Bonferroni, 1935). For multi-step indentations, multiple comparisons of short (G_{10ms}) and long term (G_∞) shear modulus were performed between indentation strains as described above. Normalized relaxation spectra for each indentation step were compared by the Kolmogorov-Smirnov statistic (Massey, 1951). A logarithmically spaced distribution of 50 data points over 20s calculated from normalized Prony series parameters were compared with the kstest2.m function in MATLAB with a Bonferroni-corrected p-value. The effect of depth on equilibrium shear modulus as measured by the AFM was evaluated with a one-way ANOVA followed by Bonferroni *post hoc* tests. For both AFM-measured storage and loss modulus, a two-way ANOVA was performed on depth and frequency followed by Bonferonni *post hoc* tests. All statistical analysis for AFM data was performed in SPSS (SPSS Inc.) and for microindenter data in MATLAB. Unless otherwise noted, a p-value of < 0.05 was considered statistically significant.

Table 1. Prony series parameters with 95% confidence intervals for all regions at 10% indentation strain.

$[G_{xx}]$ = Pa, $[\tau_{xx}]$ = s	G_∞	G_1	τ_1	G_2	τ_2	G_3	τ_3	R^2
Hippocampus CA1	226±12	802±90	0.014±0.002	275±25	0.22±0.06	213±18	4.8±1.1	0.99
Hippocampus CA3	206±16	1145±146	0.012±0.002	295±33	0.22±0.07	264±25	4.2±1.0	0.99
Dentate Gyrus	119±77	532±115	0.015±0.004	253±26	0.35±0.12	235±60	11.9±8.2	0.99
Cortex	292±20	731±75	0.018±0.003	322±28	0.33±0.09	234±24	5.9±1.8	0.99
Thalamus	179±4	750±42	0.020±0.001	362±7	1.34±0.08	-	-	0.98
Corona Radiata	175±17	1207±111	0.012±0.001	338±22	1.26±0.05	219±18	6.0±1.6	0.99
Corpus Callosum	116±6	3939±699	0.003±0.001	441±16	0.10±0.01	267±9	3.8±0.3	0.98
Brainstem	134±17	1131±184	0.009±0.002	305±21	0.24±0.05	214±17	6.1±1.6	0.99
Cerebellum (Grey)	118±9	273±18	0.066±0.010	208±15	3.48±0.67	-	-	0.93
Cerebellum (White)	136±8	744±65	0.021±0.002	329±11	1.77±0.20	-	-	0.90

RESULTS:

A displacement profile from a microindentation test is shown in Figure 1. The total ramp time was ~60 ms, and displacement was held constant for 20 s. Acceleration and deceleration required 10 ms. Signal noise due to the low reaction forces is evident but did not prevent identification of Prony series parameters. Load during the 60 ms ramp was recorded for fitting at short time scales (Figure 1b inset).

The Prony series parameters with 95% confidence intervals for an indentation strain of 10% are listed in Table 1. As determined by the F-test, relaxation behavior was captured with three decay terms for all regions except for the thalamus and cerebellum (grey and white matter), which required only two. R^2 values ranged from 0.98-0.99 for most regions (Table 1). The small loads and degree of relaxation for the cerebellum may have contributed to its lower R^2 values (0.93 and 0.90).

The shear relaxation modulus calculated from the Prony series parameters at short times (G_{10ms} and G_{50ms}) and at equilibrium (G_∞) are shown in Figure 2. The tissue relaxes quickly, by almost 70% by 50 ms. Significant differences between regions were present for a few comparisons at 10 ms including the cerebellum grey matter which was significantly different from all other regions except the dentate gyrus.

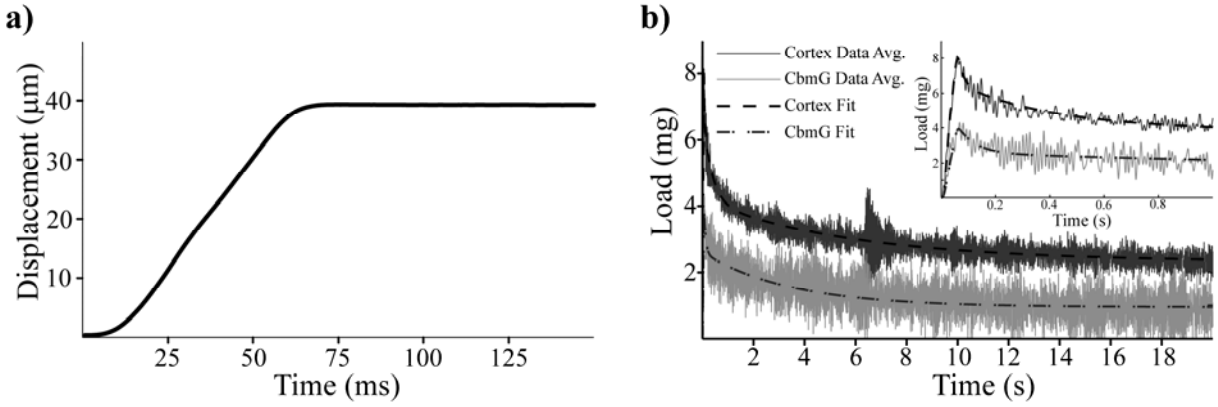

Fig. 1 - a) Measured indentation profile for a single indentation. b) Average load for a soft region (cerebellum grey matter; CbmG) and a stiff region (cortex) with the theoretical load calculated from the hereditary integral of the indenter displacement and the fit relaxation function.

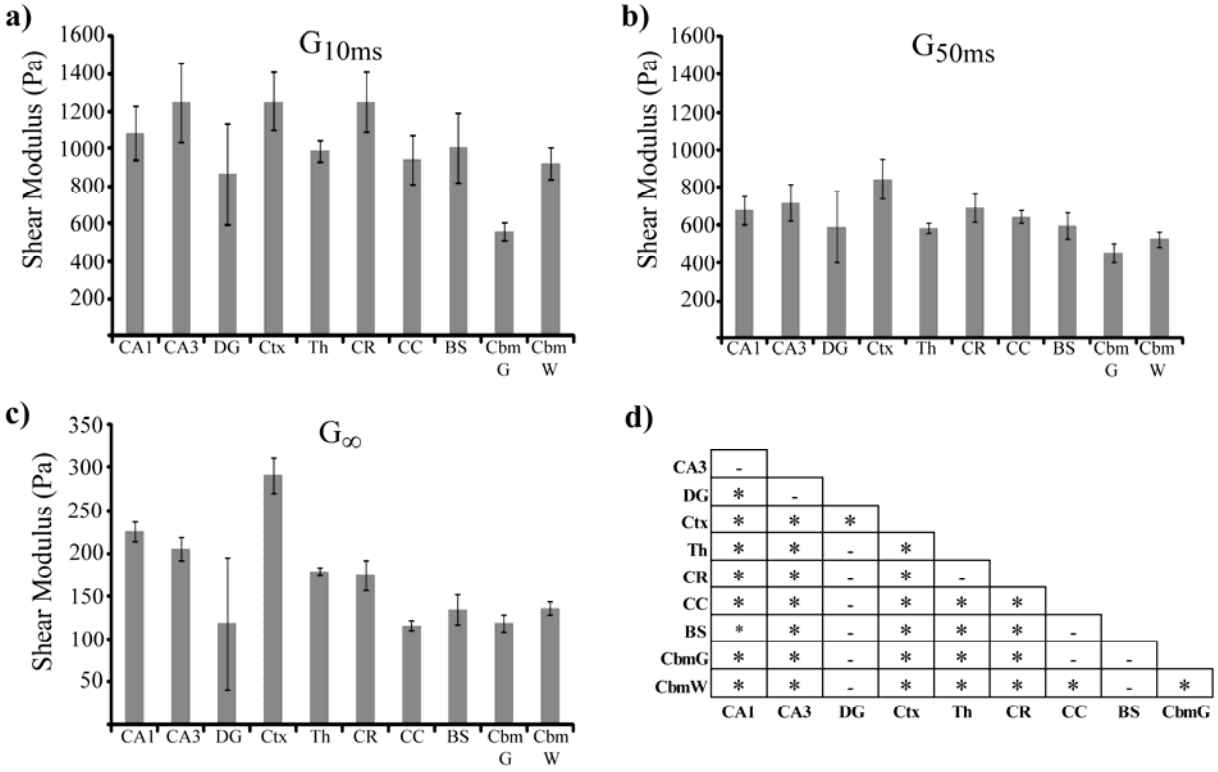

Fig. 2 - a) G_{10ms}, b) G_{50ms}, and c) G_∞ (note change in scale) from Prony series fits for each region for 10% indentation strain. d) Results from *post hoc* tests for G_∞. (*, $p < 0.05$; mean ± 95% c.i.)

At 50 ms, more regional differences exist with cortex being the stiffest region and the cerebellum the softest. These trends were consistent at equilibrium with numerous significant differences observed.

The average load for multi-step indentations in the corona radiata is shown in Figure 3a. Prony series parameters for each step individually are shown in Figure 3b. Both G_{10ms} and G_∞ increased significantly with indentation strain suggesting that tissue stiffness increased with indentation depth (Figure 3c). However, normalized relaxation spectra for each indentation were not significantly different (Figure 3d). A static deflection curve (0.01 Hz) from AFM oscillatory tests is shown in Figure 4a with the identified contact point. Average pseudo-static equilibrium modulus, G_∞, increased significantly with

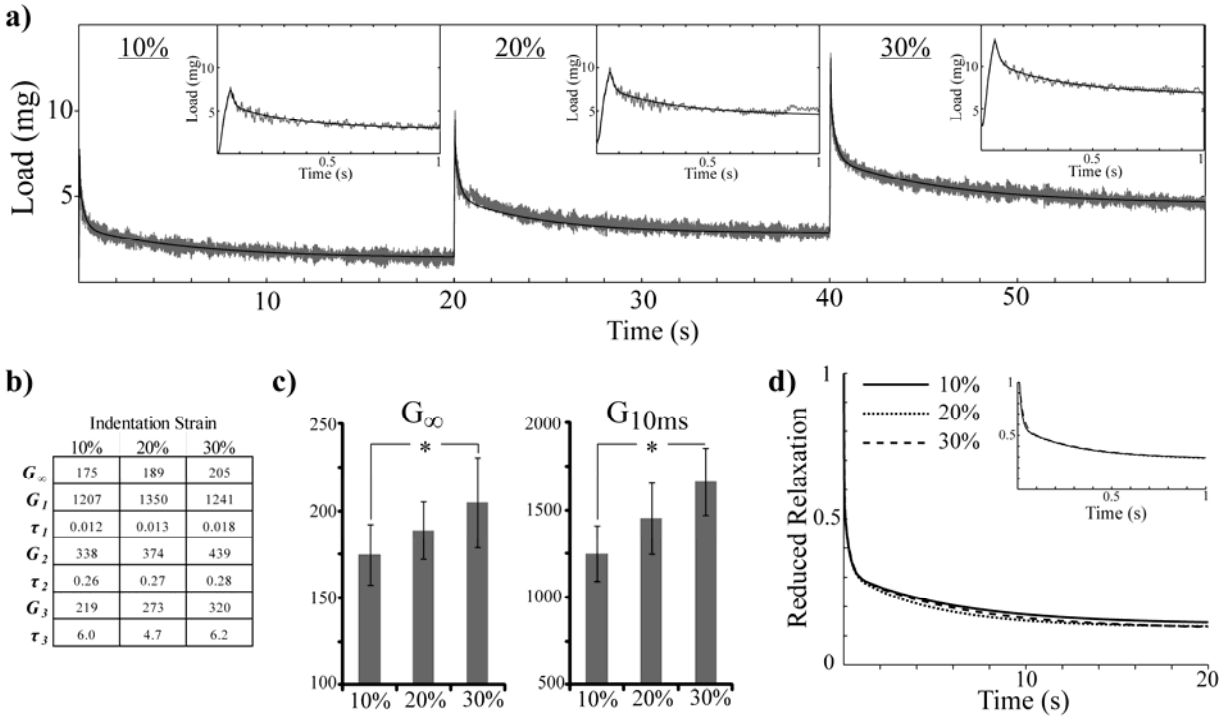

Fig. 3 - a) Average load for all three step indentations in corona radiata with Prony series fits performed at each indentation. b) Prony series fit parameters for each step analyzed individually. c) Equilibrium (G_∞) and short-term (G_{10ms}) modulus from fit parameters for each indentation (mean ± 95% c.i.). d) Reduced relaxation function normalized to G_{10ms} for each step indentation.

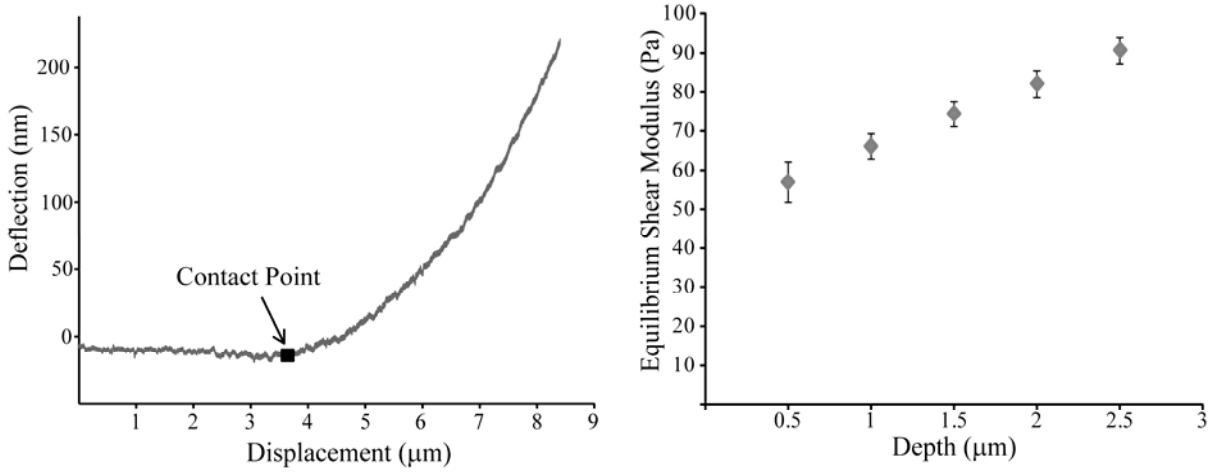

Fig. 4 - a) A force deflection curve of the slow (0.01Hz) indentation and identified contact point (■) from dynamic AFM tests. b) Average depth-dependent pseudo-static shear modulus from all indentations in the corona radiate as derived from the 0.01Hz indentation deflection histories. (mean ± s.e.m.)

indentation depth, from 58 Pa at 0.5 μm to 91 Pa at 2.5 μm (Figure 4b).

Depth dependent storage and loss modulus at each frequency is presented in Figure 5. Frequency and indentation depth were both significant factors affecting storage and loss modulus. Storage modulus increased significantly with frequency and indentation depth. Loss modulus increased significantly with frequency but decreased significantly with indentation depth at frequencies larger than 50 Hz. Storage modulus was greater than loss modulus at lower frequencies, but loss modulus generally became stiffer than storage modulus at 100 Hz.

Results from both methods were compared in both the frequency (Figure 6) and time (Figure 7) domains using correspondence principles (Equations 12 and 13). In the frequency domain, converted

microindenter storage modulus was approximately three times stiffer than the storage modulus measured by AFM (Figure 6a). Converted microindenter loss modulus was approximately two times stiffer than loss modulus measured by the AFM (Figure 6b). In the time domain, it was evident that the relaxation behavior in microindenter tests was more gradual than in AFM tests (Figure 7). However, short term modulus and long term modulus measured from both methods were consistent, within 10% for instantaneous moduli and only a two-fold difference for equilibrium modulus.

DISCUSSION:

The mechanical events of TBI that trigger the subsequent pathobiology require less than 150 ms (Kleiven and Hardy, 2002; Kleiven, 2007; Yoganandan et al., 2008). To understand the intracranial biomechanics of TBI, mechanical properties for the involved anatomical regions must be defined on the appropriate temporal scale (10s of ms) and for the appropriate strains (Takhounts et al., 2003; Takhounts et al., 2008). Porcine models of TBI have been used as surrogates to human TBI because of their

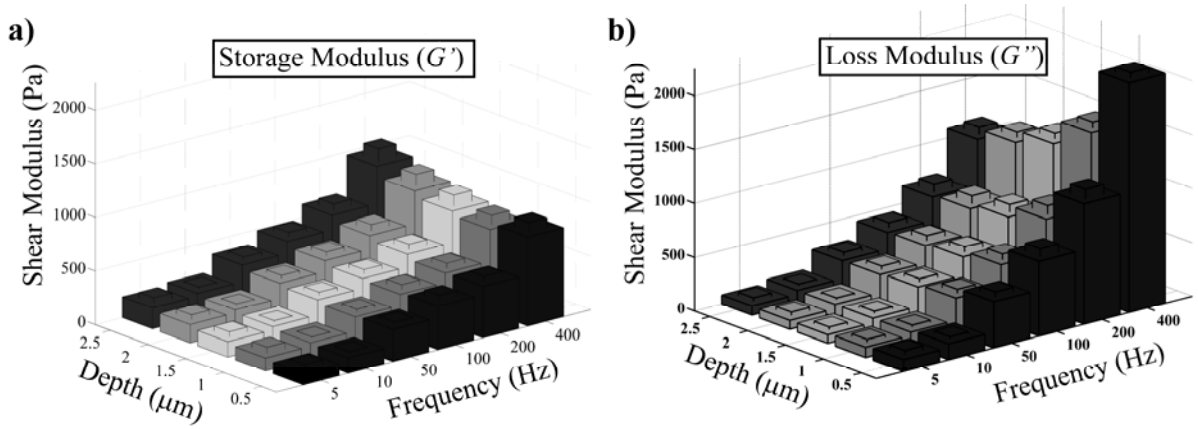

Fig. 5 - a) Storage and b) loss shear modulus as a function of depth and strain determined from AFM oscillatory tests in the corona radiata. (large bars = mean, small bars = s.e.m.)

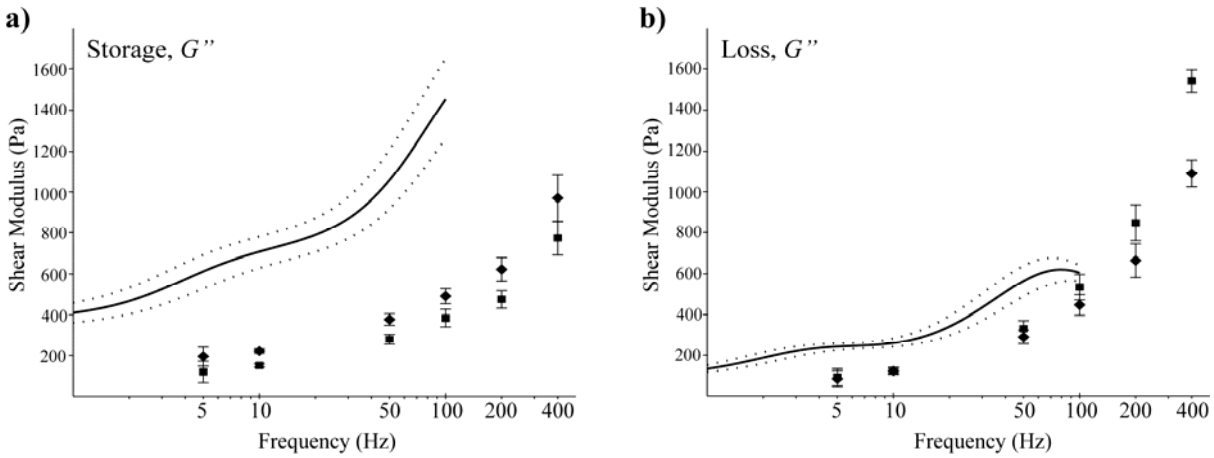

Fig. 6 - a) Storage and b) loss modulus from AFM oscillatory tests at indentation depths of 1 μm (■) and 2.5 μm (♦, mean ± s.e.m.) compared to mean (solid line) and 95% confidence interval (dotted line) of microindenter data converted to the frequency domain using Equations 12 and 13 for the corona radiata.

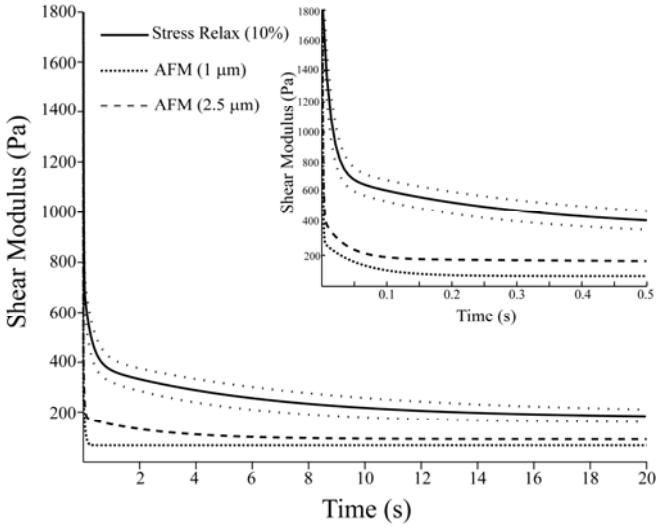

Fig. 7 - Shear relaxation modulus calculated from Prony series fit (solid black line) and 95% confidence interval (dotted) from 10% indentation strain stress relaxation tests compared to AFM data from oscillatory tests at depths of 1 μm and 2.5 μm converted to the time domain using Equations 12-14.

anatomically similar brain, large size and experimental tractability for monitoring clinically relevant physiologic parameters (Fritz et al., 2005; Manley et al., 2006). Many studies have examined the dynamic mechanical properties of porcine brain tissue to better understand the biomechanics of injury. However, large variability in results possibly due to sample preparation or post mortem time to testing have hampered interpretation of results (Hrapko et al., 2008a). In addition, many of these mechanical properties were not generated at time scales relevant to TBI (i.e. decay constants greater than 100 ms) (Prange and Margulies, 2002). Finally, traditional methods such as parallel plate shear or rheometer testing require relatively large samples which prevent characterization of homogeneous samples of small anatomic regions on a spatial scale relevant to the heterogeneous distribution of tissue damage observed upon histological examination of the tissue (Meaney et al., 1995; Sparrey et al., 2009).

Indentation testing is well-suited for measuring mechanical properties of the brain on the same spatial scale as anatomical regions. Spatial resolution is limited by the size of the indenter and the sensitivity of the force transducer. Indentation is a validated method for measuring time-dependent mechanical properties of materials (Cheng et al., 2000; Mahaffy et al., 2000; Zamir and Taber, 2004). Homogeneous samples need not be prepared as the probe can be easily positioned in a region of interest. Here, we have used two modalities and spatial scales for testing the mechanical properties of porcine brain tissue: a cylindrical microindenter with a 250 μm radius for stress relaxation tests in the time domain and an AFM with a 12.5 μm radius spherical tip probe for oscillatory tests in the frequency domain.

Single step, microindentation stress relaxation tests were performed to a depth of 40 μm (indentation strain ~10%). Because data was recorded during the indentation ramp (Figure 1), mechanical characterization at short time scales relevant to TBI was possible. The small size of the probe also facilitated the measurement of mechanical properties in both large and small anatomic regions at spatial scales not previously achieved. Short term shear modulus (G_{10ms}) ranged from 0.6 kPa to 1.2 kPa based on region. At this short time point, cortical grey and white matter (Ctx and CR respectively) did not differ however the corpus callosum was significantly less stiff. The cerebellar grey matter was the softest region at this time scale. At 50 ms (G_{50ms}), the cortex was the stiffest region and cerebellar grey matter the softest. While more significant regional differences were apparent at this time scale, the most numerous differences were observed for the equilibrium modulus (G_∞; Figure 2d).

In comparison to relaxation moduli reported in the literature, the results presented here for comparable regions were stiffer. For the cortical grey matter and white matter (Ctx, CR), thalamus, and corpus callosum, shear moduli found here were three times stiffer at 100 ms and two times stiffer

at equilibrium than those previously reported (Prange and Margulies, 2002; Coats and Margulies, 2006). These differences may be due to preconditioning that was not performed here in order to capture the mechanical properties as would be present during an initial blow to the head. The short term modulus reported here for the cortex is very close to that reported by Gefen and Margulies for non-preconditioned porcine cortex *in vivo* (1.9 kPa) while the equilibrium modulus reported here was half as stiff as that reported by Gefen and Margulies (Gefen and Margulies, 2004). For the brainstem, results presented here were softer than those reported previously and were softer than cerebral cortex which is counter to what has been reported previously (Arbogast and Margulies, 1998).

No other studies have examined the mechanical properties of the hippocampus in the porcine brain. In a previous study using the AFM to measure pseudo-static mechanical properties in the rat hippocampus, the CA1 sub region was the stiffest and the dentate gyrus was the softest region (Elkin et al., 2010). Our current results are consistent with those results (Figure 2c) which suggests that subanatomic distribution of mechanical properties may be conserved across species.

Multi-step indentation tests in cortical white matter (corona radiata; Figure 3) were used to examine the nonlinearity of brain tissue (Takhounts et al., 2003). From Prony series fits to each step indentation, both short term (G_{10ms}) and equilibrium (G_∞) modulus increased significantly with indentation strain (Figure 3c). However, the lack of significant differences between the reduced relaxation functions for each indentation step suggests that the relaxation behavior of the tissue is the same at different strains despite the strain nonlinearity. There have been conflicting results in the literature regarding the strain-time separability of brain tissue (Mendis et al., 1995; Miller and Chinzei, 1997; Bilston et al., 2001) but our results suggest that the behaviors are separable and that quasilinear viscoelastic theory (Fung, 1993) may be adequate to describe the mechanical behavior of brain under large deformation. The decrease in loss modulus at the small deformations in AFM tests does however conflict with this result and may suggest that it is only valid for larger deformations.

Dynamic AFM experiments were performed in cortical white matter (corona radiata; Figure 4 and 5). The pseudo-equilibrium modulus (G_∞; Figure 4b) and storage modulus (G'; Figure 5a) increased significantly with indentation depth, confirming nonlinear mechanical behavior. The loss modulus decreased with increasing indentation depth suggesting a transition between viscoelastic phenomenon (i.e. fluid pressurization and flow vs. matrix viscoelasticity) at different depths of indentation.

In the frequency domain, the differences between test methods were within the range of previously reported differences for the porcine corona radiata. For both methods, frequency dependent storage modulus (0.2 to 1.4 kPa) and loss modulus (0.1 to 1.6 kPa) were very similar to other studies on corona radiata and were well within the variability within the literature at similar frequencies for both storage modulus (0.2 to 5 kPa) and loss modulus (0.1 to 3 kPa) (Hrapko et al., 2008a).

Correspondence principles between the frequency and time domains were used to compare measurements (Nicolle et al., 2005; Hrapko et al., 2008b). In the frequency domain, storage and loss moduli measured with the AFM were less stiff than those converted from the time domain from stress relaxation tests (Figure 6). This difference may be due to the effects of indenter size. Brain has been described previously as a biphasic or poroelastic material composed of a solid porous matrix and a fluid phase (Mow et al., 1980; Cheng and Bilston, 2007). Given the size of the AFM probe, our oscillatory tests may be measuring components of the viscoelastic solid matrix and not the contribution of fluid flow through the matrix. In contrast, the microindenter probe, an order of magnitude larger than the AFM probe, may be measuring the combined effects of the tissue matrix *and* the flow of extracellular fluid through its pores which may better describe the macroscopic behavior of the tissue. Another possible explanation for the discrepancy in results is that microindenter tests were performed at room temperature due to instrumentation constraints while AFM tests were performed at 37ºC. Hrapko et al. have shown that the frequency-dependent complex modulus of porcine brain tissue at room temperature is more than 1.5 times stiffer than at 37ºC (Hrapko et al., 2008a). Finally, preconditioning during AFM oscillatory tests may result in the lower moduli reported from AFM data (Gefen and Margulies, 2004).

Instantaneous shear moduli converted from AFM data were within 10% of that measured with the microindenter (Figure 7). The relaxation behavior however was significantly different. The AFM-derived shear modulus relaxed much more quickly than that measured with the microindenter. Again, these discrepancies could be explained by the differences in probe size. Equilibrium and

instantaneous moduli are more strongly influenced by the tissue matrix which has effects at the short and long times whereas the relaxation behavior over 20 s is influenced by fluid flow through pores of the tissue. Such a theory explains the slower relaxation times observed with the larger probe, suggesting that microindenter results may measure mechanical behavior of the tissue more appropriate for contemporary FE models.

This study is the first to measure porcine brain tissue mechanical properties at this spatial resolution. One other recent study has examined regional differences in porcine brain mechanical properties using indentation testing. However, only relative differences between white and grey matter regions were reported, and mechanical parameters consistent with the time scale of TBI were not presented (van Dommelen et al., 2010). The spatial resolution afforded by our methods and the Prony series parameters generated herein can be used to inform new FE models containing detailed anatomic resolution. The outputs of these models could for the first time be compared to histological data on the same spatial scale.

Differences between our results and some of those in the literature may be due to several factors: 1) age-dependence of mechanical properties (Thibault and Margulies, 1998; Prange and Margulies, 2002; Elkin et al., 2010), 2) effect of post-mortem time (Fallenstein et al., 1969; Garo et al., 2007) which was under 3 h in our study, 3) bathing of tissue in a pH-balanced nutrient medium for the duration of testing, 4) time scale and magnitude of deformations were different from many other studies, and 5) indentation testing at different spatial scales may interrogate different architectural components of the tissue.

A limitation of this study is the small strain approximation used for deriving Equations 1 and 9 (Harding and Sneddon, 1945; Radok and Lee, 1960; Ting, 1966; Johnson, 1970). At large depths of indentation (i.e. > 10%), these assumptions may break down. To address this limitation, future studies will employ an inverse finite element modeling strategy to quantify their error at large indentation strains. Another limitation is that brain tissue is not isotropic especially in white matter regions with significant fiber alignment. Up to two-fold differences have been observed depending on the direction of measurement in the corpus callosum (Prange and Margulies, 2002), up to 1.3 fold differences in the corona radiata (Hrapko et al., 2008a), and up to 1.2 fold differences in the brainstem (Arbogast and Margulies, 1998). Here, indentations in only a single plane, the coronal plane, were performed, and isotropy was assumed. Future studies will address anisotropy through indentations in orthogonal planes.

CONCLUSION:

In this study we have characterized the high-rate linear viscoelastic mechanical properties of multiple anatomic regions of the adult porcine brain using a microindentation stress relaxation method. Prony series parameters were generated that can now be used to populate finite element models with mechanical property data at an appropriate anatomic resolution. The microindentation method was cross-validated at a smaller spatial scale using AFM oscillatory tests. Partial agreement of the two methods further validates the results but does suggest that the spatial scale of the measurement should be taken into account during future mechanical testing. Results from both measurement methods for the corona radiata were consistent with those in the literature which supports the validity of measurements performed in the other anatomic regions. Nonlinearity of the tissue was examined through multi-step indentations (10, 20, 30% indentation strain) in the corona radiata. The results suggest that modeling of brain tissue as a quasilinear viscoelastic material is valid and can be used in the future to further characterize the large deformation behavior of multiple anatomic regions of the brain for modeling TBI.

REFERENCES:

Alcaraz J, Buscemi L, Puig-de-Morales M, Colchero J, Baro A, Navajas D (2002) Correction of microrheological measurements of soft samples with atomic force microscopy for the hydrodynamic drag on the cantilever. Langmuir 18:716-721.

Allen MP (1997) Testing Hypotheses in Nested Regression Models. In: Understanding regression analysis, pp 113-115. New York ; London: Plenum Press.

Arbogast KB, Margulies SS (1998) Material characterization of the brainstem from oscillatory shear tests. Journal of Biomechanics 31:801-807.

Bilston LE, Liu Z, Phan-Thien N (2001) Large strain behaviour of brain tissue in shear: some experimental data and differential constitutive model. Biorheology 38:335-345.
Bonferroni CE (1935) Il calcolo delle assicurazioni su gruppi di teste. In: Studi in Onore del Professore Salvatore Ortu Carboni, pp 13-60. Rome.
Cheng L, Xia X, Yu W, Scriven LE, Gerberich WW (2000) Flat-punch indentation of viscoelastic material. Journal of Polymer Science Part B-Polymer Physics 38:10-22.
Cheng S, Bilston LE (2007) Unconfined compression of white matter. J Biomech 40:117-124.
Cheng S, Clarke EC, Bilston LE (2008) Rheological properties of the tissues of the central nervous system: A review. Medical Engineering & Physics 30:1318-1337.
Coats B, Margulies SS (2006) Material properties of porcine parietal cortex. J Biomech 39:2521-2525.
Costa KD, Yin FCP (1999) Analysis of indentation: Implications for measuring mechanical properties with atomic force microscopy. Journal of Biomechanical Engineering-Transactions of the Asme 121:462-471.
Crick S, Yin F (2006) Assessing Micromechanical Properties of Cells with Atomic Force Microscopy: Importance of the Contact Point. Biomechanics and Modeling in Mechanobiology:1-12.
Darvish KK, Crandall JR (2001) Nonlinear viscoelastic effects in oscillatory shear deformation of brain tissue. MedEng Phys 23:633-645.
Donnelly BR, Medige J (1997) Shear properties of human brain tissue. JBiomechEng 119:423-432.
Elkin BS, Ilankovan A, Morrison B (2010) Age-Dependent Regional Mechanical Properties of the Rat Hippocampus and Cortex. J Biomech Eng 121.
Fallenstein GT, Hulce VD, Melvin JW (1969) Dynamic Mechanical Properties of Human Brain Tissue. Journal of Biomechanics 2:217-&.
Fritz HG, Walter B, Holzmayr M, Brodhun M, Patt S, Bauer R (2005) A pig model with secondary increase of intracranial pressure after severe traumatic brain injury and temporary blood loss. J Neurotrauma 22:807-821.
Fung YC (1993) Biomechanics : mechanical properties of living tissues, 2nd Edition. New York: Springer-Verlag.
Garo A, Hrapko M, van Dommelen JA, Peters GW (2007) Towards a reliable characterisation of the mechanical behaviour of brain tissue: The effects of post-mortem time and sample preparation. Biorheology 44:51-58.
Gefen A, Margulies SS (2004) Are in vivo and in situ brain tissues mechanically similar? Journal of Biomechanics 37:1339-1352.
Harding JW, Sneddon IN (1945) The Elastic Stresses Produced by the Indentation of the Plane Surface of a Semi-Infinite Elastic Solid by a Rigid Punch. P Camb Philos Soc 41:16-26.
Hrapko M, van Dommelen JA, Peters GW, Wismans JS (2008a) The influence of test conditions on characterization of the mechanical properties of brain tissue. J Biomech Eng 130:031003.
Hrapko M, van Dommelen JA, Peters GW, Wismans JS (2008b) Characterisation of the mechanical behaviour of brain tissue in compression and shear. Biorheology 45:663-676.
Hyder AA, Wunderlich CA, Puvanachandra P, Gururaj G, Kobusingye OC (2007) The impact of traumatic brain injuries: a global perspective. NeuroRehabilitation 22:341-353.
Johnson KL (1970) Correlation of Indentation Experiments. Journal of the Mechanics and Physics of Solids 18:115-&.
Kleiven S (2007) Predictors for traumatic brain injuries evaluated through accident reconstructions. Stapp Car Crash J 51:81-114.
Kleiven S, Hardy WN (2002) Correlation of an FE Model of the Human Head with Local Brain Motion--Consequences for Injury Prediction. Stapp Car Crash J 46:123-144.
Lin DC, Dimitriadis EK, Horkay F (2007) Robust strategies for automated AFM force curve analysis--I. Non-adhesive indentation of soft, inhomogeneous materials. J Biomech Eng 129:430-440.
Lippert SA, Rang EM, Grimm MJ (2004) The high frequency properties of brain tissue. Biorheology 41:681-691.
Mahaffy RE, Shih CK, MacKintosh FC, Kas J (2000) Scanning probe-based frequency-dependent microrheology of polymer gels and biological cells. PhysRevLett 85:880-883.

Mahaffy RE, Park S, Gerde E, Kas J, Shih CK (2004) Quantitative analysis of the viscoelastic properties of thin regions of fibroblasts using atomic force microscopy. BiophysJ 86:1777-1793.
Manley GT, Rosenthal G, Lam M, Morabito D, Yan D, Derugin N, Bollen A, Knudson MM, Panter SS (2006) Controlled cortical impact in swine: pathophysiology and biomechanics. J Neurotrauma 23:128-139.
Massey FJ (1951) The Kolmogorov-Smirnov Test for Goodness of Fit. J Am Stat Assoc 46:68-78.
Mattice JM, Lau AG, Oyen ML, Kent RW (2006) Spherical indentation load-relaxation of soft biological tissues. Journal of Materials Research 21:2003-2010.
Meaney DF, Smith DH, Shreiber DI, Bain AC, Miller RT, Ross DT, Gennarelli TA (1995) Biomechanical analysis of experimental diffuse axonal injury. JNeurotrauma 12:689-694.
Mendis KK, Stalnaker RL, Advani SH (1995) A Constitutive Relationship for Large-Deformation Finite-Element Modeling of Brain-Tissue. Journal of Biomechanical Engineering-Transactions of the Asme 117:279-285.
Menon DK (2009) Unique challenges in clinical trials in TBI. Crit Care Med 37:S129-135.
Miller K, Chinzei K (1997) Constitutive modelling of brain tissue: Experiment and theory. Journal of Biomechanics 30:1115-1121.
Mow VC, Kuei SC, Lai WM, Armstrong CG (1980) Biphasic creep and stress relaxation of articular cartilage in compression? Theory and experiments. J Biomech Eng 102:73-84.
Nicolle S, Lounis M, Willinger R, Palierne JF (2005) Shear linear behavior of brain tissue over a large frequency range. Biorheology 42:209-223.
Ommaya AK (1968) Mechanical properties of tissues of the nervous system. JBiomech 1:127-138.
Pamidi MR, Advani SH (1978) Non-Linear Constitutive Relations for Human-Brain Tissue. Journal of Biomechanical Engineering-Transactions of the Asme 100:44-48.
Prange MT, Margulies SS (2002) Regional, directional, and age-dependent properties of the brain undergoing large deformation. JBiomechEng 124:244-252.
Radok JRM, Lee EH (1960) The Contact Problem for Viscoelastic Bodies. J Appl Mech 27:438-444.
Sakai M (2002) Time-dependent viscoelastic relation between load and penetration for an axisymmetric indenter. Philosophical Magazine a-Physics of Condensed Matter Structure Defects and Mechanical Properties 82:1841-1849.
Shuck LZ, Advani SH (1972) Rheological Response of Human Brain-Tissue in Shear. Journal of Basic Engineering 94:905-911.
Sparrey CJ, Manley GT, Keaveny TM (2009) Effects of White, Grey, and Pia Mater Properties on Tissue Level Stresses and Strains in the Compressed Spinal Cord. Journal of Neurotrauma 26:585-595.
Takhounts EG, Crandall JR, Darvish K (2003) On the importance of nonlinearity of brain tissue under large deformations. Stapp Car Crash Journal 47:79-92.
Takhounts EG, Ridella SA, Hasija V, Tannous RE, Campbell JQ, Malone D, Danelson K, Stitzel J, Rowson S, Duma S (2008) Investigation of traumatic brain injuries using the next generation of simulated injury monitor (SIMon) finite element head model. Stapp Car Crash J 52:1-31.
Thibault KL, Margulies SS (1998) Age-dependent material properties of the porcine cerebrum: effect on pediatric inertial head injury criteria. Journal of Biomechanics 31:1119-1126.
Ting TCT (1966) Contact Stresses between a Rigid Indenter and a Viscoelastic Half-Space. J Appl Mech 33:845-&.
van Dommelen JA, van der Sande TP, Hrapko M, Peters GW (2010) Mechanical properties of brain tissue by indentation: interregional variation. J Mech Behav Biomed Mater 3:158-166.
Yoganandan N, Li J, Zhang J, Pintar FA, Gennarelli TA (2008) Influence of angular acceleration-deceleration pulse shapes on regional brain strains. J Biomech 41:2253-2262.
Zamir EA, Taber LA (2004) On the effects of residual stress in microindentation tests of soft tissue structures. Journal of Biomechanical Engineering-Transactions of the Asme 126:276-283.